AERODYNAMIC ANALYSIS OF FIELD WIND TURBINE: A COMPARATIVE STUDY OF COMPUTATIONAL METHODS WITH EXPERIMENTAL VALIDATION

Vidosava VILOTIJEVIĆ [*1], Jelena SVORCAN [2], Milan ŠEKULARAC [1], Igor VUŠANOVIĆ [1], Miki HONDŽO [3]

[*1] University of Montenegro, Faculty of Mechanical Engineering, Džordža Vašingtona bb, 81000 Podgorica, Montenegro

[2] University of Belgrade, Faculty of Mechanical Engineering, Kraljice Marije 16, 11120 Belgrade, Serbia

[3] University of Minnesota, Department of Civil, Environmental, and Geo- Engineering, St. Anthony Falls Laboratory, 2nd Third Ave SE, Minneapolis 55414, United States

[*] Corresponding author; E-mail: vidosavav@ucg.ac.me

The study compares performance predictions from Blade Element Momentum Theory, Computational Fluid Dynamics methods, and experimental results for a 2.5 MW horizontal wind turbine across various wind speeds. The results indicate that Computational Fluid Dynamics or in complex flow conditions, although Blade Element Momentum Theory remains useful during the initial design stages. The analysis also underscores the influence of wind speed and shear stress transport on performance metrics such as turbine power output and flow characteristics. Despite certain modeling simplifications, such as the omission of detailed blade tip geometryies, the findings suggest that both numerical methods exhibit trends consistent with the field experimental data. The study highlights the importance of detailed simulations for optimizing wind turbine performance and outlines future research focused on noise reduction and its impact on biodiversity.

Key words*: wind turbine, Computational Fluid Dynamics (CFD), Blade Element Momentum Theory (BEMT), turbulence models.*

1. Introduction

In recent years, wind energy has rapidly become a cornerstone of the global transition to renewable energy, driven by the urgent need to reduce carbon emissions and enhance energy security. The development of larger wind turbines (ranging from one to several megawatts) has been a critical trend in the industry, as the power generated by a wind turbine increases with the square of the rotor diameter. This makes larger turbines inherently more efficient and cost-effective, especially when combined with increased turbine heights, which provide more consistent access to high wind speeds and improve the capacity factor of wind farms [1,2]. Consequently, optimizing wind turbine designs, particularly the aerodynamics of the rotor, has become crucial for maximizing energy output and reducing the levelized cost of energy [3].

The foundation of modern wind turbine aerodynamics can be traced back to the seminal works of Betz [4] and Joukovski [5], who established the theoretical limits of wind energy conversion efficiency. Building on this, Glauert [6] made a significant contribution by developing the Blade Element Momentum Theory (BEMT), which has since become a cornerstone in the design and optimization of Horizontal-Axis Wind Turbines (HAWTs). BEMT, which combines blade element theory with momentum theory, allows for the efficient prediction of aerodynamic forces on turbine blades. Despite its simplicity, BEMT has proven remarkably accurate in nominal operating conditions, making it an essential tool in the early stages of wind turbine design [7-9].

However, the assumptions underlying BEMT, such as uniform inflow and simplified blade geometry, can limit its accuracy, particularly for modern, large-scale wind turbines operating under complex flow conditions. Computational Fluid Dynamics (CFD) has emerged as a more sophisticated method for analyzing wind turbine aerodynamics to address these limitations. CFD techniques, particularly those utilizing advanced turbulence models, including the Shear Stress Transport (SST) $k-\omega$ model, offer a more detailed and accurate prediction of aerodynamic performance aerodynamic performance prediction. These turbulence models capture complex flow phenomena, including turbulence, flow separation, and wake interactions, which are critical for the design and optimization of large wind turbines [10,11].

Our study specifically aims to tackle the challenges posed by the aerodynamic analysis of a large, curved-blade wind turbine. The computational domain is vast, encompassing a wide range of length scales, from the smallest that influence turbulence to much larger scales. For example, the smallest airfoil chord length is 69.6 mm, and the largest is 3708 mm, while the total blade length is 46700 mm. Additionally, part of the domain exhibits quasi-rotational behavior, requiring significant computational resources. As a result, the calculations are time-consuming, and convergence issues may arise. This research examined a 2.5 MW Clipper Liberty C96 wind turbine, 96 m rotor diameter with 80 m hub height at the University of Minnesota's Eolos Wind Energy Research Field Station (Fig. 1) [12]. The turbine's substantial size and curved blade geometry make it an ideal candidate for evaluating the applicability of both BEMT and CFD methods. Additionally, the availability of an extensive experimental data set, collected from the field station's advanced sensor systems provides a unique opportunity for rigorous validation of BEMT and CFD methods. The data was used to examine the power dependence on wind speed, turbine efficiency via the power coefficient, and the wind-to-tip speed ratio. These variables are critical attributes commonly used in wind turbine design.

Figure 1. 2.5 MW Clipper Liberty C96 wind turbine, University of Minnesota.

The primary objective of this study is to perform a comparative analysis of BEMT and CFD methods, with a particular focus on their ability to accurately predict the aerodynamic performance of the turbine under different wind conditions. By validating the simulation results against the experimental data, the research aims to assess the strengths and limitations of each method, especially in the context of large, curved blade geometries and the applicability of various turbulence models. The findings of this study will contribute to the ongoing efforts to optimize wind turbine designs, ultimately enhancing the efficiency and sustainability of wind energy systems.

2. Metodology

The blade geometry schematic with forces acting on the blade is shown in Fig. 2. The blade is divided into 47 airfoils, which can be categorized into three main groups. Starting from the center of rotation, the first six airfoils are circular, enabling a smooth transition from circular to Delft University (DU) airfoil shapes. The next 35 airfoils belong to the group of DU airfoils, covering 80% of the blade. The last six airfoils form the C-96 blade tip. The direction of rotation, as well as the thrust T, drag D, and lift L forces acting on the blade, are shown in Fig. 2.

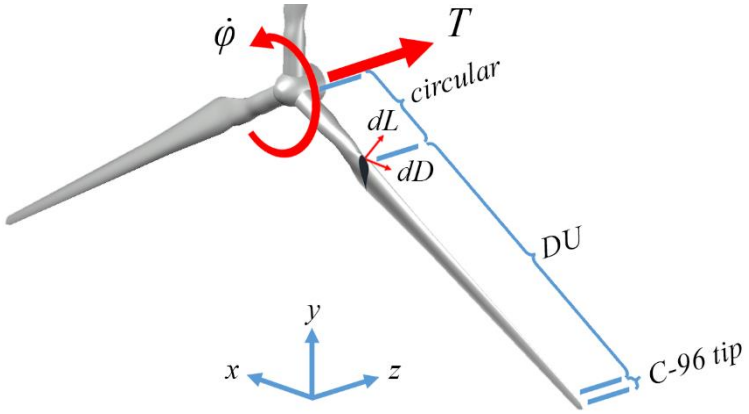

Figure 2. Blade geometry schematic with forces acting on the blade.

For an annular ring at radius a r [m] with differential thickness dr, infinitesimal change of thrust T [N] is:

$$dT = 4\pi\rho r u^2 a(1-a)dr, \tag{1}$$

where ρ [kg/m^3] represents the air density, u [m/s] is the free stream speed, and a stands for the axial induction factor:

$$a = \frac{u_i}{u}, \tag{2}$$

where u_i [m/s] is the axial velocity.

The total thrust T value is obtained by summing (numerically integrating) along the blade/disc.

The power extracted by the rotor P [W] can be expressed as:

$$P = T \cdot u + 2\pi\rho \int_0^R r u^2 a(1-a)dr, \tag{3}$$

where R [m] is the blade/disc radius.

The fluid flow around the wind turbine (Fig. 1) simulations were performed using ANSYS Fluent [13] and QBlade [14]. The ANSYS software performs calculations by discretizing the Navier-Stokes equations using the Finite Volume Method (FVM). Being based on the BEMT method, the QBlade software calculates wind turbine aerodynamic performance, including lift, drag, thrust, and power coefficients. Numerical results were compared with the field data.

2.1. Blade Element Momentum Theory computational model

The Blade Element Momentum Theory (BEMT) model combines two theories, Momentum Theory, and Blade Element Theory, to predict the forces acting on propellers or turbines. Momentum Theory uses the conservation of momentum and energy to determine the velocity and pressure of the fluid through the propeller or turbine disk. It assumes the disk produces a pressure jump that leads to a change in momentum in the fluid. Blade Element Theory divides the blades of the propeller or turbine into small elements along the radius. Each element is analyzed separately, using aerodynamic principles, to determine the lift and drag forces acting on that element. For a blade element at radius r with chord length c [m], the differential lift dL [N] and drag dD [N] are given by:

$$dL = \frac{1}{2}\rho v^2 c C_L dr, \tag{4}$$

$$dD = \frac{1}{2}\rho v^2 c C_D dr, \tag{5}$$

where v [m/s] is the relative velocity at the blade element, while C_L and C_D represent the lift and drag coefficients, respectively. The relative velocity v at the blade element is a combination of the axial and tangential components:

$$v = \sqrt{(u(1-a))^2 + (\Omega r(1+a'))^2}, \tag{6}$$

where Ω [s^{-1}] is the angular speed, and a' is the tangential induction factor.

The angle of attack α is given as a difference between a flow angle ϕ and a pitch angle of the blade θ, while the flow angle ϕ can be obtained from:

$$\tan\phi = \frac{u(1-a)}{\Omega r(1+a')}. \tag{7}$$

The differentials of a thrust dT and a torque dQ [Nm] for a blade element are given as:

$$dT = B\left[\frac{1}{2}\rho v^2 c\left(C_L\cos\phi + C_D\sin\phi\right)\right]dr, \tag{8}$$

$$dQ = B\left[\frac{1}{2}\rho v^2 c\left(C_L\cos\phi - C_D\sin\phi\right)\right]dr, \tag{9}$$

where B is the number of blades.

Rapid iterations in the early stages of turbine design are necessary to allow quick testing of different parameters, such as blade shape, length, and angle of attack, to assess their impact on performance and ensure that the turbine meets performance, efficiency, and cost goals before committing to more detailed, time-consuming analyses. For this purpose, BEMT model's efficiency makes it preferable choice. Recent studies have affirmed that BEMT can produce results with a high degree of accuracy comparable to more complex CFD methods [15]. This makes it especially valuable when computational resources are limited or quick assessments are needed [16].

2.1.1 Computational procedure for Blade Element Momentum Theory model

The blade is divided into 47 segments along its span for the wind turbine shown in Fig. 1. Each segment represents a cross-sectional blade slice. This discretization level allows for a detailed analysis of the blade's aerodynamic performance and structural behavior. An appropriate DU airfoil profile is selected for each segment based on the blade design. The airfoil data is manually entered into the analysis software. The local angle of attack, and the lift and drag forces are computed. The forces calculated for each segment are then integrated along the blade span to determine the overall aerodynamic forces and moments on the blade. Once the individual blade analysis is complete, the results are integrated into a full rotor analysis, considering the interaction between blades and other components of the wind turbine. By detailing the above steps, it's clear that the analysis, while systematic, involves considerable manual input and attention to detail, especially when dealing with a large number of cross-sections. Precision in data entry, careful selection of airfoil profiles, and iterative refinement are crucial to achieving accurate and reliable results using the BEMT method.

2.2. The Finite Volume Method

The Finite Volume Method (FVM) is applied to discretize and solve the governing equations for fluid flow, and other related phenomena. The fundamental equations include the continuity and momentum equations (Navier-Stokes equations), and energy equations. The differential form of the momentum equation is converted into an integral form over a control volume V giving:

$$\int_V \frac{\partial(\rho\vec{u})}{\partial t}dV + \int_S \rho\vec{u}(\vec{u}\cdot\vec{n})dS = -\int_S p\vec{n}dS + \int_S \vec{\tau}\cdot\vec{n}dS + \int_V \Phi dV, \tag{10}$$

where t [s] is the time, $\vec{n}$ is the outward normal unit vector, p [Pa] is the air pressure, $\vec{\tau}$ [N/m^2] is the stress tensor, Φ [N/m^3] are the body forces, such as the gravity and centrifugal force, and S is surface of the control volume.

Reynolds-Averaged Navier-Stokes (RANS) turbulence models are a class of models used to simulate turbulent flows by averaging the Navier-Stokes equations, which describe the motion of fluid. These models introduce additional terms to represent the effects of turbulence, which must be modeled using turbulence closure models. In this paper, two Reynolds turbulence models are employed for the shear stress transport (SST), including SST $k-\omega$ and the SST transition models.

The SST $k-\omega$ model is a widely used in CFD. It effectively predicts flow separation under adverse pressure gradients and provides accurate results for a wide range of applications, including aerospace and automotive engineering. The following equations formulate the SST $k-\omega$ turbulence model:

$$\frac{\partial}{\partial t}(\rho k)+\frac{\partial}{\partial x_j}(\rho v_j k)=\frac{\partial}{\partial x_j}\left(\left(\mu+\frac{\mu_t}{\sigma_k}\right)\frac{\partial k}{\partial x_j}\right)+\mu_t S^2-\rho\beta^* k\omega, \tag{11}$$

$$\frac{\partial}{\partial t}(\rho\omega)+\frac{\partial}{\partial x_j}(\rho v_j \omega)=\frac{\partial}{\partial x_j}\left(\left(\mu+\frac{\mu_t}{\sigma_\omega}\right)\frac{\partial \omega}{\partial x_j}\right)+\frac{\alpha}{\nu_t}\mu_t S^2-\rho\beta\omega^2+D_\omega\left(\omega,\frac{\partial k}{\partial x_j},\frac{\partial \omega}{\partial x_j}\right), \tag{12}$$

where k [J/kg] is the turbulent kinetic energy, ω [s^{-1}] is the specific dissipation rate, x_j [m] is the spatial coordinate, v_j [m/s] is the component of velocity vector, μ [Pa·s] is the dynamic viscosity of the fluid, μ_t [Pa·s] is the turbulent viscosity, ν_t [m^2/s] is the kinematic turbulent viscosity, σ_k is the turbulent Prandtl number for k, σ_ω is the turbulent Prandtl number for ω, S [s^{-1}] is the strain rate magnitude, α, β and β^* are the model constants, and D_ω is the cross-diffusion therm that improves accuracy near walls.

On the other hand, the SST transition model is an extension of the SST $k-\omega$ model that incorporates transition modeling capabilities. This model accounts for the transition from laminar to turbulent flow, which is crucial for accurately predicting the behavior of boundary layers and the onset of turbulence. The inclusion of transition effects improves the prediction accuracy for flows with significant laminar-turbulent transition regions, such as those encountered in turbine blades, airfoils, and other aerodynamic surfaces. This model is based on the following equations:

$$\frac{\partial}{\partial t}(\rho\gamma)+\frac{\partial}{\partial x_j}(\rho v_j\gamma)=\frac{\partial}{\partial x_j}\left(\left(\mu+\frac{\mu_t}{\sigma_\gamma}\right)\frac{\partial \gamma}{\partial x_j}\right)+P_\gamma-E_\gamma, \tag{13}$$

$$\frac{\partial}{\partial t}(\rho \mathrm{R\tilde{e}}_{\theta t})+\frac{\partial}{\partial x_j}(\rho v_j \mathrm{R\tilde{e}}_{\theta t})=\frac{\partial}{\partial x_j}\left(\sigma_{\theta t}\left(\mu+\frac{\mu_t}{\sigma_\gamma}\right)\frac{\partial \mathrm{R\tilde{e}}_{\theta t}}{\partial x_j}\right)+P_{\theta t}, \tag{14}$$

where: γ is the intermittency factor, σ_γ is the model constant related to the diffusion of intermittency, $\mathrm{R\tilde{e}}_{\theta t}$ is the momentum-thickness Reynolds number, $\sigma_{\theta t}$ is the model constant related to $\mathrm{R\tilde{e}}_{\theta t}$, P_γ and $P_{\theta t}$ are the production terms, and E_γ is the rate of energy dissipation.

2.2.1 Simulation setup for Finite Volume Method approach

The rotor is positioned within a cylindrical computational domain representing the air in which the rotor operates. This domain is divided into a rotating region (around the rotor) and a stationary region (the far-field surrounding fluid). The Moving Reference Frame (MRF) Method is employed. The rotor is modeled within the MFR while the surrounding fluid is stationary. The MRF method simplifies the problem by transforming the equations of motion into the rotating frame, which reduces the computational cost and complexity. However, it assumes a steady-state rotation, which may not fully capture transient effects. The simulation layout was arranged to describe an isolated rotor with a

diameter of $D = 96\,\text{m}$. The computational domain has the shape of a cylinder with a diameter of $3D$ and a height of $4D$. The rotor is placed distance of 1D from the inlet and is centered in the spanwise direction (Fig. 3).

The grid (Fig. 4) was created using ANSYS Fluent Mesher. Computational mesh is generated for the entire domain, with a finer mesh near the rotor blades, to capture the intricate flow details, and a coarser mesh further away. Local refinements of the grid were performed to capture the complex shape of the blade. The coarse mesh scale is on the order of 15 m, while the fine mesh scale is approximately $2 \cdot 10^{-5}$ m. Also, the airfoils at the very tip of the blade are up to 50 times smaller in chord length compared to the other airfoils. This imbalance in dimensions presents a significant challenge when modeling the mesh. Given the hardware resources available during the research, refining the mesh to that extent was not feasible, so the blades were simulated without the tips. The unstructured grid was formed and it has 8,590,896 elements and 3,470,566 nodes. A uniform velocity field was assumed at the inlet. The simulation was conducted for wind speeds ranging from 4 to 12 m/s. Based on the tip speed ratio, the rotational speeds for the wind speeds used are in the range of 1.0627 to 1.6224 rad/s. The simulation is conducted as quasi-stationary, using the SST $k-\omega$ and SST transitional Reynolds turbulence models. The quasi-stationary numerical approach involves modifying the flow equations in the region of the domain corresponding to the rotor (around the blades) by adding inertial terms due to rotation. Thus, there is no physical rotation or alteration of the computational grid during the calculation.

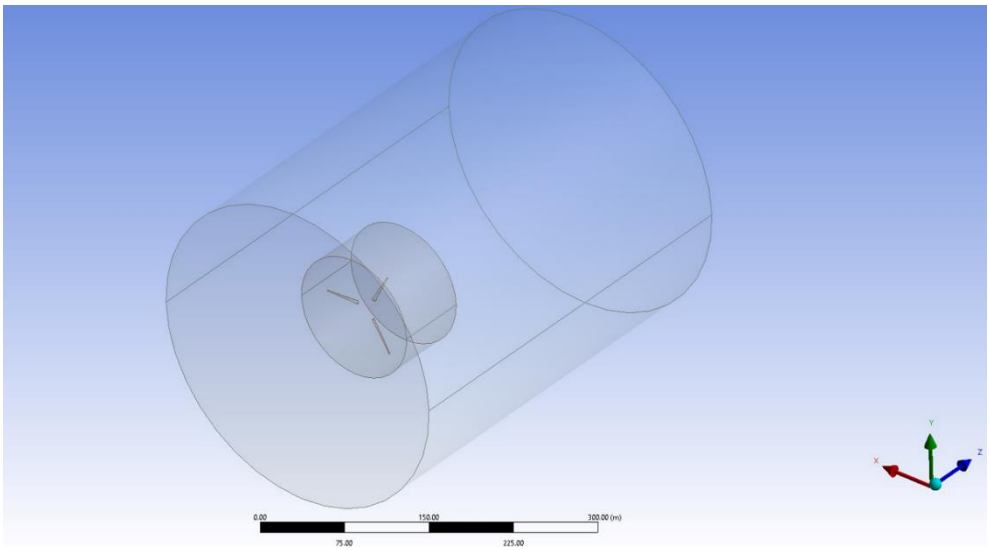

Figure 3. Computational domain with wind turbine blades.

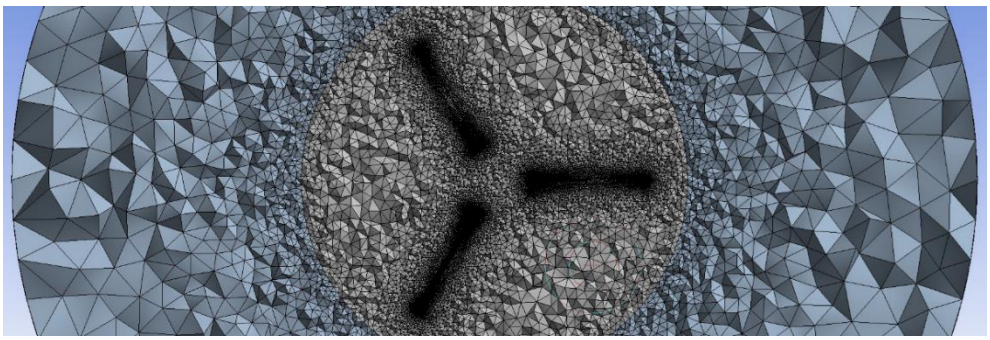

a)

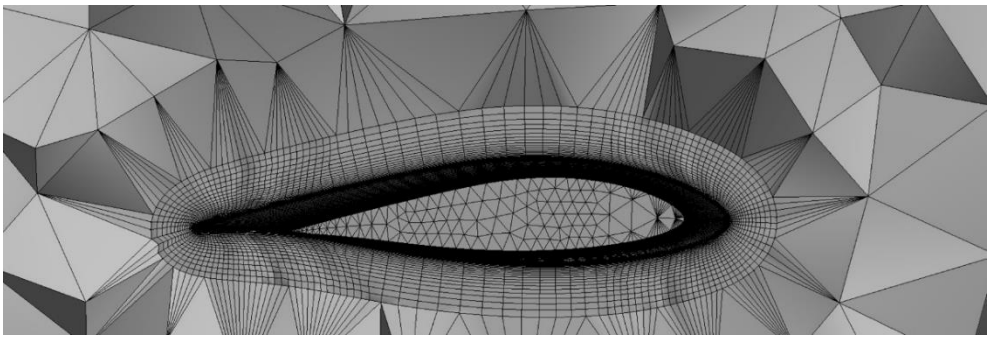

b)

Figure 4. Computational mesh: a) on the rotor and stator, b) over the boundary layer.

The convergence of the model output by varying the number of computational elements is investigated (Fig. 5). Meshes of different densities were created, and the calculated power coefficients (obtained as the ratio of the actual power output of the turbine to the total available power in the wind passing through the area swept by the turbine blades) were compared to the measured values. The mean value of the relative error for each wind speed analyzed quantifies the difference between the computed and measured power coefficients. The analysis suggests an approximately constant relative error of the power coefficient (11%) for the number of computational elements larger than $7 \cdot 10^6$.

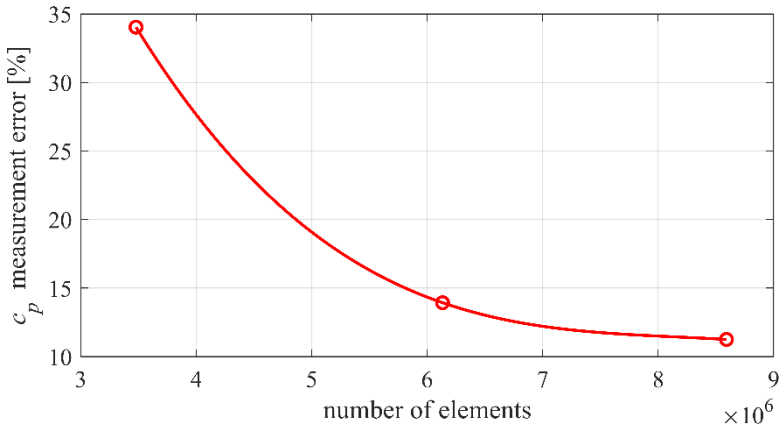

Figure 5. The error of power coefficient c_p versus number of computational elements.

3. Results and Discussion

This paper demonstrates the results obtained from simulations using two different turbulence models, along with results from QBlade simulations, and compares them with experimental data. The simulation results provide detailed insights into the performance and behavior of the wind turbine under various wind conditions. The impact of different wind speeds (ranging from 4 to 12 m/s) on the turbine's power is quantified and presented in Fig. 6. The SST $k-\omega$ and SST transitional Reynolds turbulence models were utilized to capture the turbulence effects more accurately. While the BEMT model prediction results in a relative error of 16%, the SST $k-\omega$ and SST transitional models are more accurate, yielding relative errors of 12.6% and 12.5%, respectively.

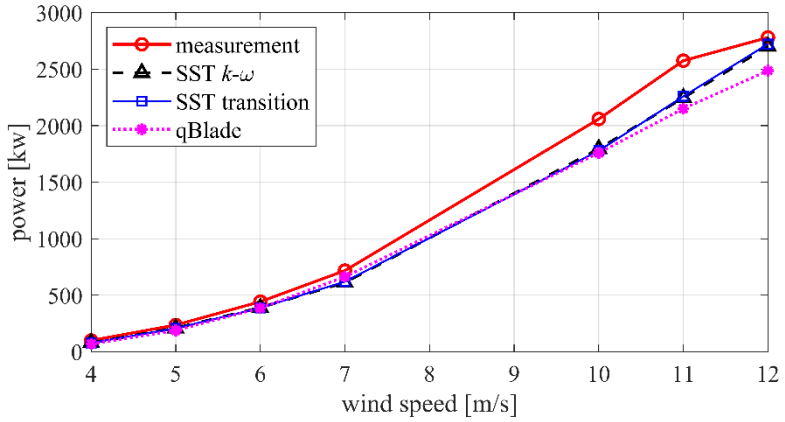

Figure 6. Measured and computed turbine generator power versus wind speed.

The relationship between the power coefficient and the tip speed ratio is illustrated in Fig. 7. Wind speed varied from 4 to 14 m/s, and the rotational speed was also varied. Overall, the three simulations underpredict the c_p, yielding the same relative errors as with the (previous) power estimation. The results obtained from CFD simulations using two different turbulence models are nearly identical. Due to the large dimensions of the turbine, a possibly insufficiently fine mesh (in relation to small turbulence structure), and the use of a quasi-stationary approach to solving the rotating flow field, both turbulence models yield very similar results.

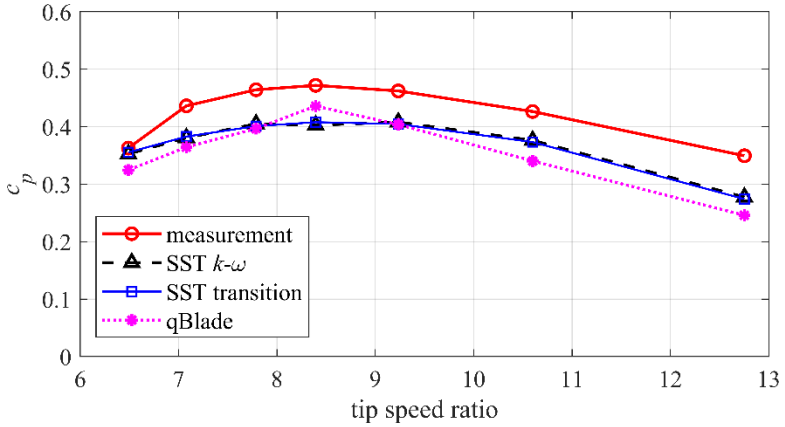

Figure 7. Power coefficient versus tip speed ratio.

Based on the data obtained, it can be concluded that experimental and numerical results exhibit the same trend in the function. The relative difference between CFD and experimental results is 12-14%. This difference primarily arises due to the modeled geometry. In numerical calculations, a simplified geometry was used because generating a mesh with the original geometry, including a curved tip, was extremely challenging. The results differ due to the assumption of a uniform velocity field at the inlet in the simulations, which is not the case in reality since the velocity profile varies significantly with height due to the atmospheric boundary layer. Additionally, the simulations ignore the influence of gravity, and structural deflections/deformations of slender wind turbine blades. The complex behavior of the scapula's structure remains inadequately understood due to limited knowledge of its internal composition, hindering the ability to fully analyze its mechanical performance. While centrifugal forces may slightly alleviate the bending induced by aerodynamic loads, the aeroelastic effects do not significantly impair overall aerodynamic performance. By

examining the curve that shows the relationship between the power coefficient and the tip speed ratio, obtained from QBlade, it is apparent that the overall trend of the function is similar. However, the numerical values differ due to the simpler model used in BEMT. One reason for the discrepancy between the numerical and experimental results is the simplification of the blade geometry at the top.

Figure 8 illustrates the variation of the thrust coefficient concerning the tip speed ratio. At lower tip speed ratio values (around 4), the thrust coefficient is approximately 0.4. As the tip speed ratio increases, the thrust coefficient steadily rises, indicating that the rotor generates more thrust at higher rotational speeds (relative to the wind speed). This force component does not contribute to the generation of torque (which is produced by the tangential forces). Still, it is crucial for the structural design of the wind turbine's tower, as these forces must be withstood, especially as they increase with wind speed.

The pressure distribution around the airfoil in the cross-section of the wind turbine blade is displayed in Fig. 9. On the upper surface of the airfoil, there is a region with lower pressure (blue/green colors). This low-pressure area is responsible for generating lift according to Bernoulli's principle. On the lower surface, the pressure is relatively higher (yellow/green colors), which further contributes to the lift generated by the airfoil. The regions of high and low pressure, combined with the airfoil shape, create a lift force that acts perpendicular to the direction of the oncoming air. The pressure distribution suggests that the airflow is accelerating over the top of the airfoil, causing the pressure to decrease (as seen by the blue regions). There are also regions of higher pressure in front of and below the airfoil (shown in red/orange), indicating air compression. This visualization is essential in understanding aerodynamic performance and optimizing airfoil shapes for various applications.

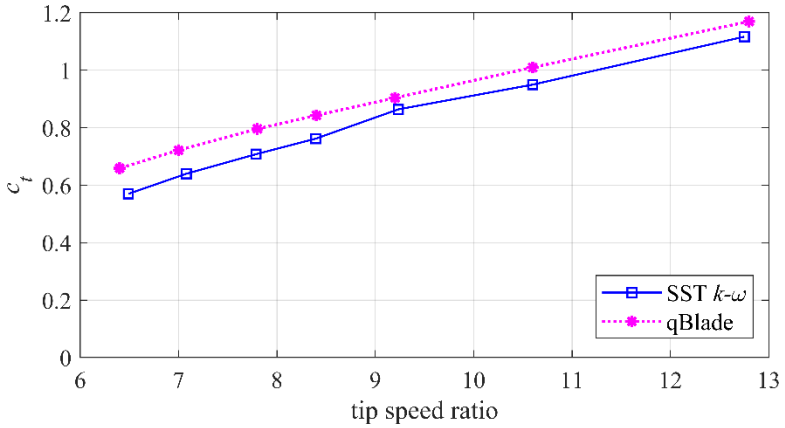

Figure 8. Thrust coefficient versus tip speed ratio.

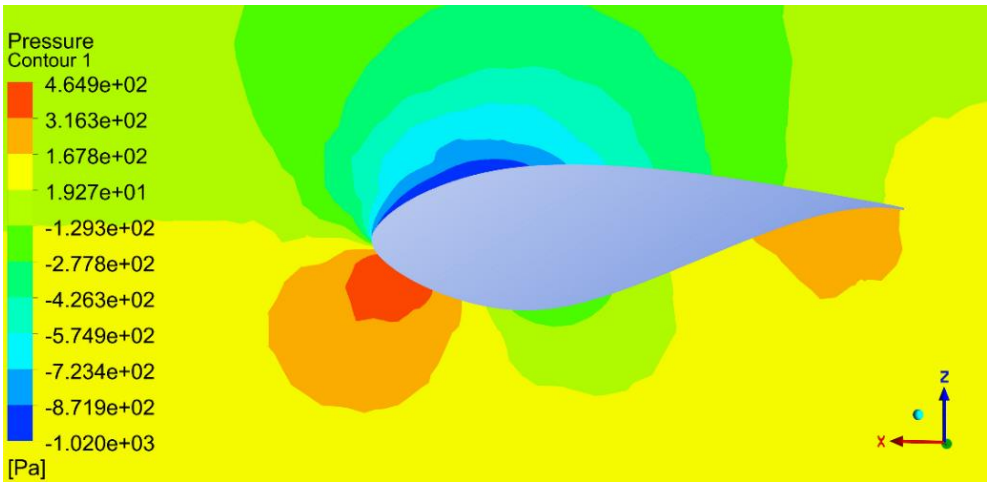

Figure 9. Pressure contours on the blade section walls of 15 m from the center of the rotor.

The w velocity (z-direction) contour, commonly used in CFD to visualize the velocity distribution in the flow field aft of the rotor, is depicted in Fig. 10.

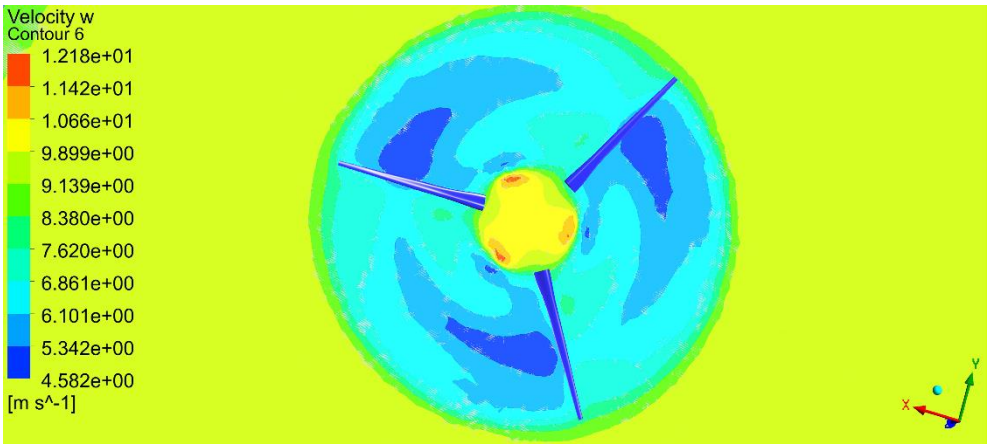

Figure 10. Velocity distribution behind the blades.

The oncoming wind's deceleration can be seen in the wake's evolution and expansion. The portion of the blade (approx. 40-90% of blade span) that contributes most to power generation can also be visualized.

4. Conclusion

This study comprehensively analyzed a large wind turbine's aerodynamic performance using CFD simulations and BEMT, comparing these with experimental data collected from the University of Minnesota's Eolos Wind Energy Research Field Station. The combination of CFD and BEMT methods, supported by experimental validation, provides a robust framework for advancing wind turbine technology, contributing to the broader goal of sustainable and reliable renewable energy generation. The study provides detailed insights into wind turbine performance under various conditions, highlighting the impact of wind speed and the effectiveness of different turbulence models. The results demonstrate that modern simulation tools can accurately predict wind turbine behavior, aiding in designing and optimizing efficient wind energy systems. The key performance metrics, such

as power coefficients and flow characteristics around the blades, were evaluated. The results showed how the uniform velocity field assumption at the inlet influenced these metrics.

This comparison between simulations and experimental field measurements was instrumental to validate the simulation models and provided insights into potential areas for improvement. The accuracy and reliability of the SST $k-\omega$ and SST transitional Reynolds models in predicting the turbine's performance were assessed. The local refinements in the grid allowed for a detailed examination of the blade's aerodynamics. The unstructured grid, with 8,989,999 elements and 345,758 nodes, enabled precise modeling of the complex blade shapes.

The quasi-stationary approach was evaluated for its effectiveness in simulating real-world conditions. SST $k-\omega$ and SST transitional Reynolds models produced results with an 87.5% overlap with the measurement data, which is very good, but could be further improved with better mesh refinement and inclusion of the blade tip geometry. Since this analysis was undertaken primarily to explore the potential for creating a net structure, the impact of blade tips on aerodynamic performance is considered negligible at this stage. However, their importance is recognized, and their role will be considered in greater detail in future studies. To accomplish this, more powerful computational resources will be required to handle the increased demands effectively. On the other hand, the BEMT model shows an 84% overlap with the measurement data. However, significantly more precise results cannot be expected from this model due to the inherent simplifications it involves. Overall, the simulation results demonstrate the intricate interplay between wind speed, rotational speed, and turbulence in determining the wind turbine's performance.

More accurate results were obtained through CFD calculations, which remain more reliable under non-optimal working conditions. However, the large and complex dimensions, irregular geometry, and wide range of scales make the calculations challenging. The findings highlight the importance of detailed aerodynamic modeling and provide a foundation for future efforts, including investigating wind turbine noise generation and its impact on biodiversity. By addressing this often-overlooked environmental factor, the subsequent research will aim to enhance the sustainability of wind energy systems to further enhance the sustainability of wind energy systems further, ensuring they not only meet energy demands but also minimize their ecological footprint.

Nomenclature

a – axial induction factor, [-]
a' – tangential induction factor, [-]
c – chord length, [m]
c_p – power coefficient, [-]
c_t – thrust coefficient, [-]
C_D – drag coefficents, [-]
C_L – lift coefficient, [-]
k – turbulent kinetic energy, [J/kg]
T – thrust, [N]
u – free stream velocity magnitude, [m/s]
v – blade element relative velocity, [m/s]
μ – dynamic viscosity of the fluid, [Pa·s]
μ_t – turbulent viscosity, [Pa·s]
ρ – air density, [kg/m^3]
ω – specific dissipation rate, [s^{-1}]
Ω – angular speed, [s^{-1}]
CFD – Computational Fluid Dynamics
DU – Delft University
BEMT – Blade Element Momentum Theory
MRF – Moving Reference Frame
RANS – Reynolds-Averaged Navier-Stokes
SST – Shear Stress Transport

References

[1] Manwell, J. F., *et al*., *Wind Energy Explained: Theory, Design and Application*, John Wiley & Sons Ltd, Chichester, United Kingdom, 2009
[2] Jonkman, J., *et al*., *Definition of a 5-MW Reference Wind Turbine for Offshore System Development*, National Renewable Energy Laboratory, Golden, Colorado, USA, 2009
[3] ***, Global Energy Transformation: A Roadmap to 2050, International Renewable Energy Agency, https://www.irena.org/publications/2019/Apr/Global-energy-transformation-A-roadmap-to-2050-2019Edition
[4] Betz, A., *Wind-Energie und ihre Ausnutzung durch Windmühlen (Wind energy and its utilization through windmills, in German)*, Vandenhoeck & Ruprecht, Goettingen, Germany, 1920
[5] Joukovski, V., *Theoretical Studies on the Aerodynamics of Wind Turbines*, 1920
[6] Glauert, H., *The Elements of Aerofoil and Airscrew Theory*, The University Press Cambridge, Cambridge, United Kingdom, 1948
[7] Sørensen, J. N., Aerodynamic Aspects of Wind Energy Conversion, *Annual Review of Fluid Mechanics, 43* (2011), 1, pp. 427-448, doi: 10.1146/annurev-fluid-122109-160801
[8] Sørensen, J. N., *General Momentum Theory for Horizontal Axis Wind Turbines*, Springer, Cham, Switzerland, 2016
[9] Sørensen, J. N., Aerodynamic Analysis of Wind Turbines, *Comprehensive Renewable Energy, 2* (2022), pp. 172-193, doi: 10.1016/B978-0-12-819727-1.00127-8
[10] Abobark, A. T., *et al*., Computational Fluid Dynamics (CFD) Investigation of NREL Phase VI Wind Turbine Performance Using Various Turbulence Models, *Processes, 12* (2024) 9, doi: 10.3390/pr12091994
[11] Pajčin, M. P., *et al*., Comparative analysis of numerical computational techniques for determination of the wind turbine aerodynamic performances, *Thermal Science, 25* (2021), 4A, pp. 2503-2515, doi: 10.2298/TSCI200216175P
[12] Eolos Wind Research Station, "Eolos Wind Research Station," University of Minnesota, [Online]. Available: https://eolos.umn.edu/eolos-wind-researchstation
[13] ANSYS® [version 18], ANSYS, Inc. Available at: https://www.ansys.com
[14] Marten, D., Wendler, J., QBlade: An Open Source Tool for Design and Simulation of Horizontal and Vertical Axis Wind Turbines, *International Journal of Emerging Technology and Advanced Engineering, 3* (2013), 3, pp. 264-269, Available at: https://qblade.org
[15] Hércules, A. O., *et al*., Assessment of Correction Methods Applied to BEMT for Predicting Performance of Horizontal-Axis Wind Turbines, *Sustainability, 15* (2023), 8, pp. 7021, doi: 10.3390/su15087021
[16] Sithole, T., *et al*., Optimizing Small Wind Turbine Blades: A BEMT Approach, *International Journal of Energetica, 8* (2023) 2, pp. 36-43

RECEIVED DATE: 30.9.2024.
DATE OF CORRECTED PAPER: 20.10.2024.
DATE OF ACCEPTED PAPER: 04.11.2024.